Foamed-metal reinforced material: tribological behaviours of foamed-copper filled with polytetrafluoroethylene and graphite

Keju Ji[1,2], **Yanqiu Xia**[1]*, **Hongling Wang**[1], and **Zhendong Dai**[2]†

[1]State Key Laboratory of Solid Lubrication, Lanzhou Institute of Chemical Physics, Chinese Academy of Sciences, Lanzhou, People's Republic of China

[2]Institute of Bio-inspired Structure and Surface Engineering, Academy of Frontier Science, Nanjing University of Aeronautics and Astronautics, Nanjing, People's Republic of China

Abstract: A novel foamed copper based (FCB) composite is developed as a rubbing pair material. The composites consist of the foamed copper and solid lubricants, such as polytetrafluoroethylene and graphite. Four kinds of FCB composites were fabricated by vacuum filtration, compression moulding, and sintering process in an orderly manner. The thermal and electrical conductivities and tribological properties of the new composites were investigated. Because the interconnected metal skeletons have been embedded in the polymers, the FCB composites possess excellent thermal and electrical conductivities, including nice self-lubricating property. The friction and wear properties were investigated on an M-2000 friction and wear tester. An electric field was imposed between the sample and ring to monitor the tribo-chemical reaction and formation of transfer film by means of 'contact resistance'. The measurements of friction temperatures were carried out by means of three thermocouples embedded in the material. The friction tests show that the friction coefficients of the FCB composites decrease almost monotonically with the increase of graphite content under different conditions; and the wear rates decrease overall compared with that of the homologous polymers, more obvious especially under severe conditions. The optical microscope, SEM, and XPS were adopted to study the worn surface morphologies and the transfer films. The main wear mechanism of the new composite is a three-body abrasion, caused and promoted by the plastic deformation, abrasive wear, and fatigue spalling. The oxidation of copper is the dominant chemical processes which occurred during the sliding process.

Keywords: foamed copper, self-lubricating composites, friction material, thermal conductivity, electrical conductivity, wear mechanisms

1 INTRODUCTION

In friction systems, the increasing demand for materials with good thermal conductivity and/or electrical has led to the quick development of advanced materials. These materials, each possessing advantages in different aspects, have found their way to the lubrication-related fields [1–4], such as brake pads, electrical brush, and sliding bearings. However, it is complicated to balance and optimize the mechanical, frictional, thermal, and electrical properties of such materials in many special cases. For instance, the continuity of substrate hard-phases was interrupted by solid lubricants, which spontaneously reduced the material strength and wear resistance; the low-melting lubricant was partially burnt or oxidized at high sintering temperatures, which may adversely affect the lubricating performance [5, 6]; the effective lubrication area was enslaved to the compactness of solid lubricants and the pore structure [7]; the conductivity values of composites presented vast differences among matrixes of various kinds, and so on.

Corresponding authors: State Key Laboratory of Solid Lubrication, Lanzhou Institute of Chemical Physics, Chinese Academy of Sciences, Lanzhou 730000, People's Republic of China.
email: xiayanqiu@yahoo.com
†*Institute of Bio-inspired Structure and Surface Engineering, Academy of Frontier Science, Nanjing University of Aeronautics and Astronautics, 29 Yudao Street, Nanjing 210016, People's Republic of China.*
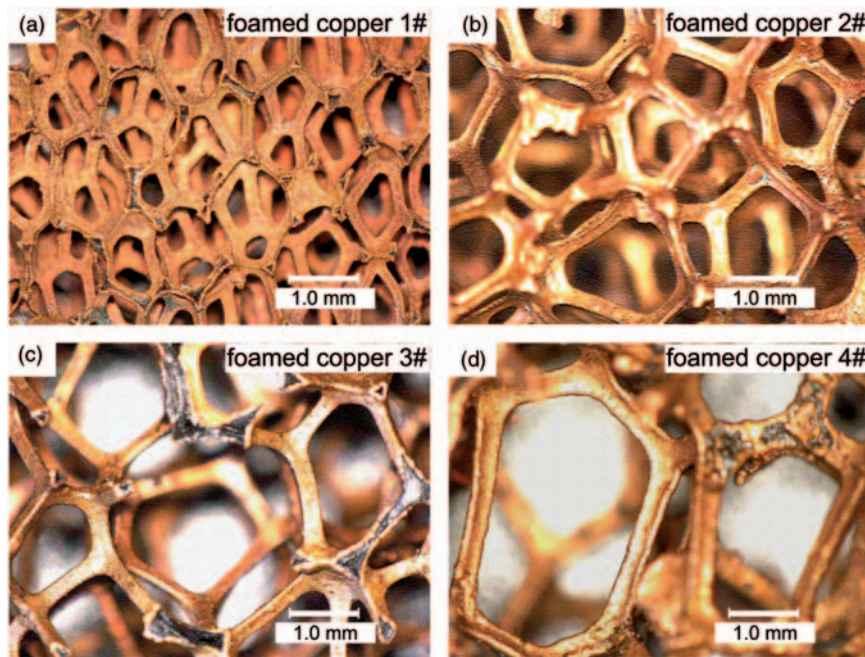*email: zddai@nuaa.edu.cn*

Fig. 1 Optical micrographs (50×) of four kinds of open-cell foamed copper (a) foamed copper 1#; (b) foamed copper 2#; (c) foamed copper 3#; and (d) foamed copper 4#)

Foamed metals, traditionally classified as closed- and open-cell, have been found attractive to be used in many industrial applications as their manufacturing methods rapidly develop [8]. By virtue of their idiosyncratic property combination of low density, specific mechanical properties, high specific surface area, and high energy absorption capability, foamed metals can, for instance, be applied in heat transformation of heat sinks, high-capacity anode materials of lithium-ion batteries, electrochemical catalysis, filters, and some other electrochemical processes like production of chlorine and its byproducts, and the elimination of volatile organic compounds as structured supports [9, 10].

Foamed copper, one kind of foamed metals, is characterized by a highly porous cell structure, large ductility, as well as extraordinary thermal and electrical conductivities. Qu et al. [11] discussed the wear characteristics of novel graphitic foam materials, and proposed three primary tribological advantages: (1) they can efficiently remove frictional heat, (2) their natural porosity can trap wear debris, and (3) their porosity can serve as a lubricant reservoir for the contact surface. Wang and Liu [12] observed that the porous metal ceramic preforms with interpenetrated network were infiltrated by Pb–Sn-based solid lubricants, and pointed out that the resultant composite has good mechanical and tribological properties. Therefore, it is worth introducing foamed copper to the tribology-related field, especially lubricating materials requiring superior electric and thermal

conductivities, better supplementary grease lubrication, as well as better performance in severe working conditions. This research described here introduces the foamed copper to tribology and represents a new approach in producing self-lubricating metal–polymer composites with an interpenetrating network. The structural composites are obtained by filling the open pores of metal foam with a polymer. The polytetrafluoroethylene (PTFE) was selected as the polymeric material due to its excellent chemical resistance, high temperature stability, and very low friction coefficient [13–19]. Meanwhile, the graphite was used as an assistant lubricant to evaluate the performance of the foamed copper based (FCB) composites well.

2 EXPERIMENTAL WORK

2.1 Materials

Four kinds of foamed copper (Ashby Materials Corporation, Shanghai, China) used in the current test have open-celled structures composed of dodecahedron-like cells, pentagonal or hexagonal faces, and hollow metallic struts, as shown in Fig. 1. Characteristics and mechanical parameters of foamed copper are given in Table 1.

PTFE and graphite, both in the form of powder, were used in making the sample. The PTFE powder (Shanghai Electrochemical Plant) has an average

Table 1 The characteristic parameters of the foamed copper

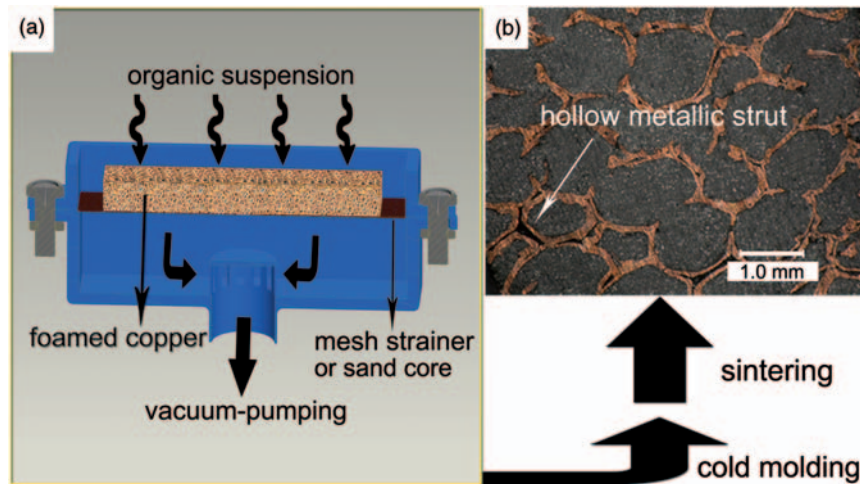| Designation	Average aperture (mm)	Porosity (%)	Pores per inch	Density (g/cm^3)	Relative density	Compressive strength (MPa)
1#	0.96	93	28	0.62	0.07	1.76
2#	1.50	96	18	0.35	0.04	0.52
3#	1.82	97	15	0.25	0.03	0.45
4#	2.88	98	10	0.24	0.03	0.36

Fig. 2 Preparation of specimens and light micrographs (50×) from the FCB composite (P/G30-1) showing surface morphology (P/G30: 70% PTFE + 30% graphite; P/G30-1: foamed copper 1# filled with component P/G30)

particle size of 60 μm and graphite flake powder (Shanghai Colloid-Chemical Plant) 7 μm.

2.2 Preparation of specimens

Foamed copper samples prepared in suitable size using bench saw or wire cutting machine were pre-treated in petroleum ether and dilute hydrochloric acid solution to remove oil and oxide on the surface. The FCB composites were fabricated by vacuum filtration, compression moulding, and sintering process in an orderly manner in the following way: first, solid lubricants according to different ratio schemes of A–E were mixed in volatile organic solution (e.g. ethanol), respectively, by magnetic stirrer. Second, the organic suspension was filled into the foamed copper sample with the help of vacuum filtration apparatus (Fig. 2). The apparatus consisted of a filter flask with a fine mesh strainer (300 meshes) or a sand core (average aperture 15–40 μm) and a vacuum pump which connected the filter flask. In the process, a flexible pipe was specially used for imbibing the suspension of solid lubricants and splashing it into the foamed copper sample, while the organic solvent was filtered out with the help of a vacuum pump (Fig. 2(a)). The filtering process took about 4 h to sufficiently volatilize ethanol to here. The filling process was completed when the bottom interspaces of foamed copper adjacent to the mesh strainer were filled up because the filling was actually a powder deposition process in interspaces from bottom to top. Afterwards, the specimens were performed with the compression moulding at 60 MPa (the same pressure with the homologous polymers) for about 5 min to allow the preparation of rectangular and cylindrical samples of dimensions $6 \times 7 \times 30$ mm^3 and $\varnothing 12.5 \times 2$ mm^2 at room temperature. The pressure here was chosen at 60 MPa because the compressive strengths of the initial foams were less (Table 1). The subsequent hardness measurements showed that the samples had similar hardness values with the ones without foamed copper. Finally, these composite blocks were sintered at 330°C for 60 min and 370°C for 60 min in the sintering furnace, and then freely cooled to room temperature. In the process of cold moulding, the foamed copper acting as the role of porous support was compacted and combined with the solid lubricant fillers, and the average compressibility in the process was up to 45 per cent of its original size compared with the initial foamed copper without fillers to 90 per cent.

In this study, five kinds of materials with different rates of compositions were filled into the foamed copper materials, respectively; at the same time, the

Table 2 Composition (vol.%) of PTFE composites

Materials	Designation	Characteristics of filler materials
100% PTFE	PTFE	PTFE powder average
90% PTFE + 10% graphite	P/G10	particle size 60 μm
80% PTFE + 20% graphite	P/G20	Graphite flake powder
70% PTFE + 30% graphite	P/G30	average particle
60% PTFE + 40% graphite	P/G40	size 7 μm

Table 3 Densities of the selective specimens

Specimen	PTFE	P/G30	P/G30-1	P/G30-2	P/G30-3	P/G30-4
Density (g/cm³)	2.16	2.18	3.21	2.82	2.73	2.66

P/G30: 70% PTFE + 30% graphite; P/G30-1: foamed copper 1# filled with P/G30 component, and so on.
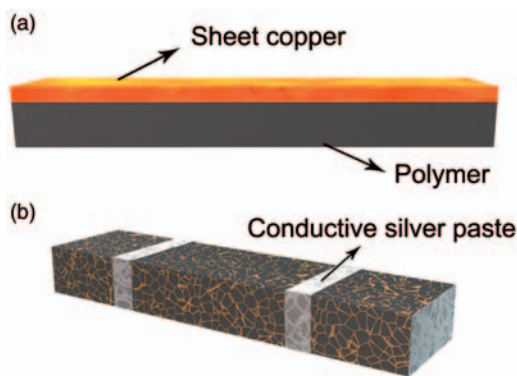

Fig. 3 Schematic diagram of the equivalent substitution of the FCB composite (a) and a key sample preparation step for the DC Kelvin Bridge test (b)

homologous PTFE-based polymers were also researched as a contrast. The compositional details of each material are listed in Table 2. Also, the densities of some selective specimens are given in Table 3.

Figure 2(b) shows surface morphology of one FCB composite (P/G30-1) before wear testing. In this photomicrograph, it can be seen that the interspaces of foamed copper were effectively crammed with solid lubricants. What is noteworthy is that the hollow metallic struts of foamed copper, widely distributed throughout the body, are expected to be helpful in storing lubricants in interfacial friction.

The cured samples were finally used for the tests of thermal and electrical conductivities and tribological capability.

2.3 Experimental

2.3.1 Electrical resistivity testing

An equivalent substitution was used to calculate the electrical resistivity of the FCB composite (Fig. 3(a)). It is defined as follows: the mass of substitute (m_0) is

equal to that of the FCB composite, m_1 refers to the mass of the upper sheet copper, the same mass as the foamed copper, m_2 to the mass of the lower polymer, A_1 and A_2 the copper and polymer densities, respectively, R_1 and R_2 the copper and polymer resistances, respectively, and ρ_1 and ρ_2 the electrical resistivities of copper and polymer, respectively.

Then, the electrical resistivity, ρ, could be calculated from the definition

$$\rho = \frac{\rho_1 \rho_2 [m_1 A_2 + (m_0 - m_1)A_1]}{\rho_1 (m_0 - m_1)A_1 + \rho_2 m_1 A_2} \quad (1)$$

Also, then, a DC Kelvin Bridge test is applied as evidence to demonstrate the effectiveness and validity of the proposed model and method. The specimens were evenly coated on both lateral faces and the potential contact areas with the conductive silver paste in order to increase the contact area in the sample preparation stage (Fig. 3(b)).

2.3.2. Friction and wear testing

The friction and wear behaviours of specimens sliding against the AISI 52100 steel in a block-on-ring configuration were investigated on an M-2000 friction and wear tester. Figure 4 shows the contact configuration of the frictional pair. The friction and wear tests were selectively conducted at a load of 100–900 N at velocities 0.424 and 0.856 m/s. The testing duration ranged from 1 to 60 min. Before each test, the surfaces of the specimen and counterpart ring were polished with no. 1000 grade SiC abrasive paper to a surface roughness of 0.08–0.15 μm. The ambient temperature was roughly 20°C and the relative humidity about 20 per cent. The friction force was measured with a torque shaft, and the friction coefficient was calculated and recorded by a computer linked with sensor. The wear rate of the specimen was determined by measuring the lost volume of sample after the friction process under applied load and sliding distance. The wear scar width was measured by a vernier caliper and three repeated trials were conducted for each sample.

Using the formula expressed below, the wear rate of each specimen was obtained

$$W = \frac{V}{LN} \quad (2)$$

where L is the velocity multiplied by the time of the friction process (s) refers to the distance of the friction (m), N to the load (N), and V the wear volume loss (mm³) having the relationship

$$V = B\left[\frac{\pi R^2}{180} \arcsin\left(\frac{b}{2R}\right) - \frac{b}{2}\sqrt{R^2 - \frac{b^2}{4}} \right] \quad (3)$$
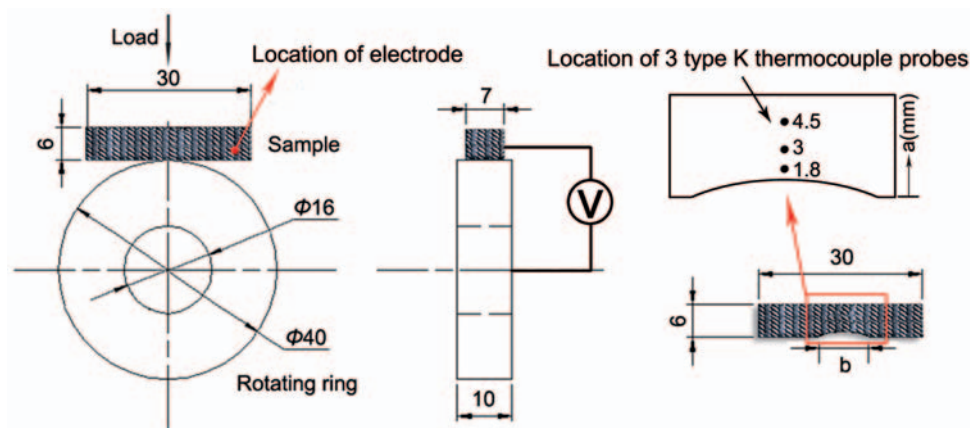
Fig. 4 Schematic diagram of M-2000 friction and wear tester and calculations of wear rate, temperature rise field, and contact resistance
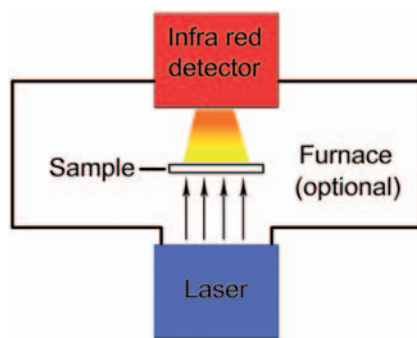

Fig. 5 Schematic diagram of LFA 447 NanoFlash

where B refers to the width of the block specimen (7 mm), R the outer radius of the steel ring (20 mm in this trial), and b the width of the wear scar (mm) [20].

The worn surface morphologies of specimens and the transfer films formed on the surfaces of the counterpart steel rings were observed on the scanning electron microscope (SEM, JSM-5600LV, Jeol, Japan) and digital microscope (VHX-600 E, Keyence, Japan).

2.3.3. Thermal conductivity and friction heat testing

The efficiency of the heat exchange and dissipation capacity of each composite was characterized by the thermal diffusivity using a testing apparatus (LFA 447 NanoFlash, Netzsch, Germany). The simplified schematic for the apparatus is shown in Fig. 5. The xenon flashlamps fire a pulse at the lower surface of the sample, while the infrared detector measures the temperature rise of the top surface of sample. The thermal diffusivity of the sample is then determined by the sophisticated software. Specific heat is measured by comparing the actual temperature rise of the sample to a temperature rise of a reference sample of known specific heat. The instrument can simultaneously measure thermal diffusivity (α) and specific heat (C_P). The software uses these values and the bulk density (ρ) to calculate thermal conductivity (λ) from the Laplace equation

$$\lambda = \alpha * C_P * \rho \qquad (4)$$

The FCB specimens in size $\varnothing 12.5 \times 2 \, \text{mm}^2$ were made by the vacuum filter, compression moulding, and sintering technique as mentioned above, while the ones without foamed copper were made just by the compression moulding and sintering technique. Two specimens were used per immersion time, and each experimental point was obtained as an average reading of three laser shots per temperature and per specimen.

Several researchers have investigated the distribution of temperature in the friction pairs [21–23]. The friction heat is generated not only on the surface of the sliding pair, but also on the bulk of the rubbing polymer material, as a result of internal friction. The highest temperature occurred inside the polymer material, at some distance from the friction surface. Wieleba [24] found that the place where the maximum temperature occurred inside the steel or polymeric element could be 1.5 mm from the surface. In order to facilitate comparison, the measurements of friction temperatures were carried out by means of thermocouples, which were embedded in the material (Fig. 4). Three 3 mm deep, 0.32 mm inner diameter holes were drilled at axial locations of 1.8, 3, and 4.5 mm as measured from the surface. These holes receive thermocouples for temperature measurement and estimation of the two-dimensional temperature field in a region beneath the contact.

3 RESULTS AND DISCUSSION

3.1 Electrical resistivity analysis

The comparison of the electrical resistivities of P/G30 Series specimens and the graphite is given in Table 4. By comparing the measured data from the DC Kelvin Bridge test with the calculated data, the theoretical analysis results are proved. Numerically, the electrical resistivity of the sample has a dramatic reduction when the foamed copper is brought in, especially the P/G30-1, compared with the polymer P/G30 (0.82 Ωm) and the pure PTFE ($\geqslant 1 \times 10^{15}$ Ωm). The low electrical resistivity of the specimen is attributed to the conductive networks formed by the interconnected metal skeleton construction, and the smaller the average aperture of foamed copper, the lower the resistance of composite.

3.2 Friction and wear behaviour

3.2.1 Effect of graphite content on the friction and wear properties of specimens

Figure 6 shows the friction coefficient and wear rate of the FCB composites and PTFE-based polymers as a function of graphite content at a velocity of 0.424 m/s

Table 4 Electrical resistivity of the selective specimens

Specimen	P/G30-1	P/G30-2	P/G30-3	P/G30-4	Graphite
Electrical resistivity ($\times 10^{-7}$ Ωm)	1.26	1.82	2.64	3.41	110

P/G30: 70% PTFE + 30% graphite; P/G30-1: foamed copper 1# filled with P/G30 component, and so on.

at a load of 500 N. It is seen that the friction coefficients of the FCB composites decrease almost monotonically with the increase of graphite content. The wear rates of the FCB composites are approximately in the following order: composites 1# FCB < 2# < 3# < 4#, while the friction coefficients are relatively complex. The lowest friction coefficients are demonstrated by the composition with 10 per cent graphite to the homologous polymers, 40 per cent to the FCB composites; and as regards to wear rates, the lowest results are obtained with 20 per cent graphite to the homologous polymers and 30 per cent to the FCB composites. The addition of graphite improves the compactness of PTFE well and decreases the ductility of PTFE-based composites, which is consistent with viewpoints of many researchers [25]. The foamed copper here serves as the supporting skeleton for polymeric matrix. Its natural porosity can trap wear debris and serve as a lubricant reservoir for the contact surface.

3.2.2 Effect of applied load on the friction and wear properties of specimens

Figure 7 shows the friction coefficient and wear rate values of the PTFE-based polymer P/G20 and FCB composite P/G30 series as a function of applied load at a velocity of 0.424 m/s. It is seen from Fig. 7(a) that the friction coefficients of the specimens decrease with the increase in load under dry friction conditions and the friction coefficients of FCB composites decrease rapidly more with increasing applied load than that of polymer P/G20. Furthermore, the friction coefficients of the FCB composites are approximately higher in an applied load range between 100 and 500 N and lower between
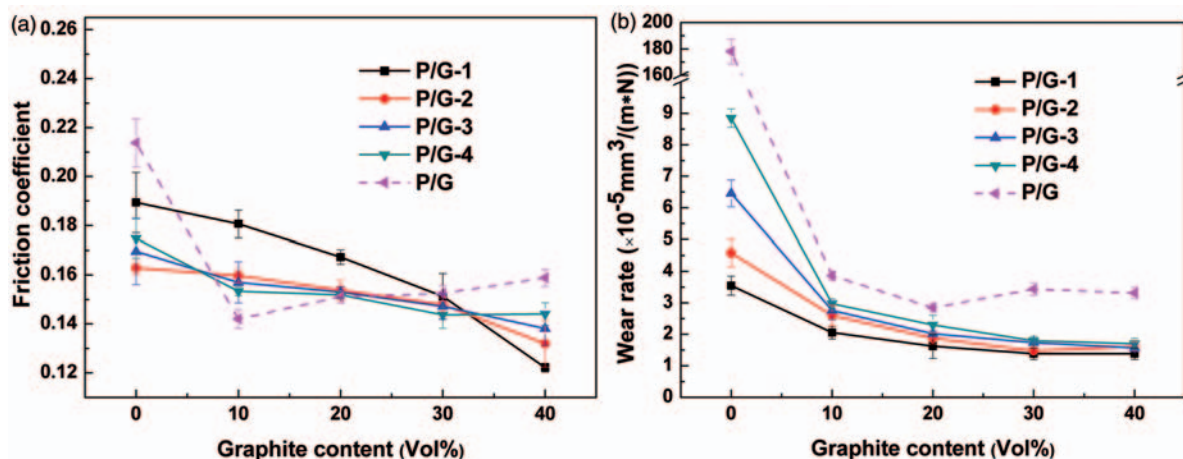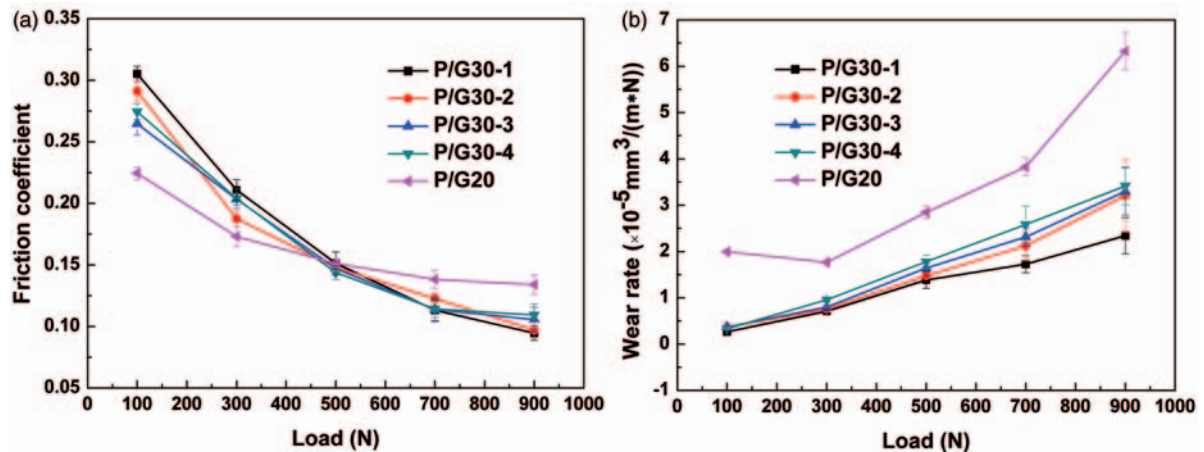

Fig. 6 Friction coefficient (a) and wear rate (b) of the FCB composites and the PTFE-based polymers as a function of graphite content at a velocity of 0.424 m/s at a load of 500 N (P/G-1~4: foamed copper 1~4# filled with component PTFE + *x*% graphite, respectively)

Fig. 7 Friction coefficient (a) and wear rate (b) of the polymer P/G20 and FCB composites as a function of applied load at a velocity of 0.424 m/s (P/G20: 80% PTFE + 20% graphite; P/G30: 70% PTFE + 30% graphite; P/G30-1: foamed copper 1# filled with P/G30 component; P/G30-2: foamed copper 2# filled with P/G30 component, and so on)
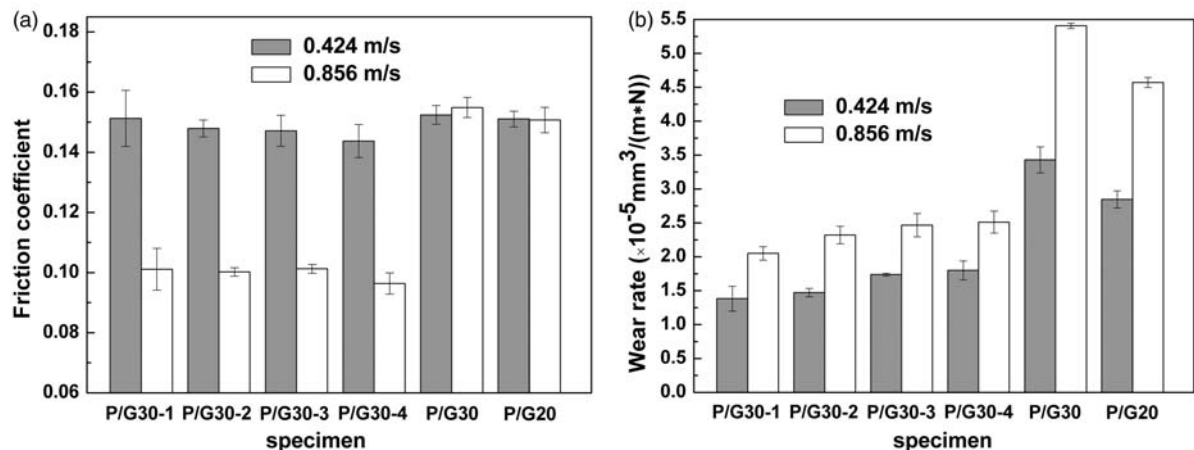

Fig. 8 Values of the friction coefficient (a) and wear rate (b) of specimens at linear velocities 0.424 m/s and 0.856 m/s at a load of 500 N (P/G20: 80% PTFE + 20% graphite; P/G30: 70% PTFE + 30% graphite; P/G30-1: foamed copper 1# filled with P/G30 component; P/G30-2: foamed copper 2# filled with P/G30 component, and so on)

500 and 900 N than that of polymer P/G20. Also, the friction coefficients decrease with the increase of average apertures of foamed copper when the applied load is less than about 600 N, compared with a contrary tendency when the load is over 600 N. Figure 7(b) reveals that the wear rates of the FCB composites increase comparatively in a slow manner with the increase of load, and the values are lower than those of polymer P/G20 at all applied loads. It also can be seen that the wear rates of the FCB composites decrease along with the decrease of average apertures of foamed copper. The preferable wearing quality benefits from the favourable thermal conduction and the hollow metallic struts of the foamed copper, which are effective in the load spread and heat distribution.

3.2.3 Effect of velocity on the friction and wear properties of specimens

Variations in the friction coefficients and wear rates with velocity for selective specimens at an applied load of 500 N are shown in Fig. 8. It can be seen from Fig. 8(a) that the friction coefficients of FCB composites P/G30 series at the higher velocity 0.856 m/s are much lower than the values achieved at the lower velocity 0.424 m/s, while the results of polymer P/G20 and P/G30 are insensitive to the velocity variations. Figure 8(b) shows that the wear rates of these selective specimens are greater at 0.856 m/s than at 0.424 m/s, and the anti-wear properties of the FCB composites are better than that of the homologous polymers at the two linear velocities. The PTFE and
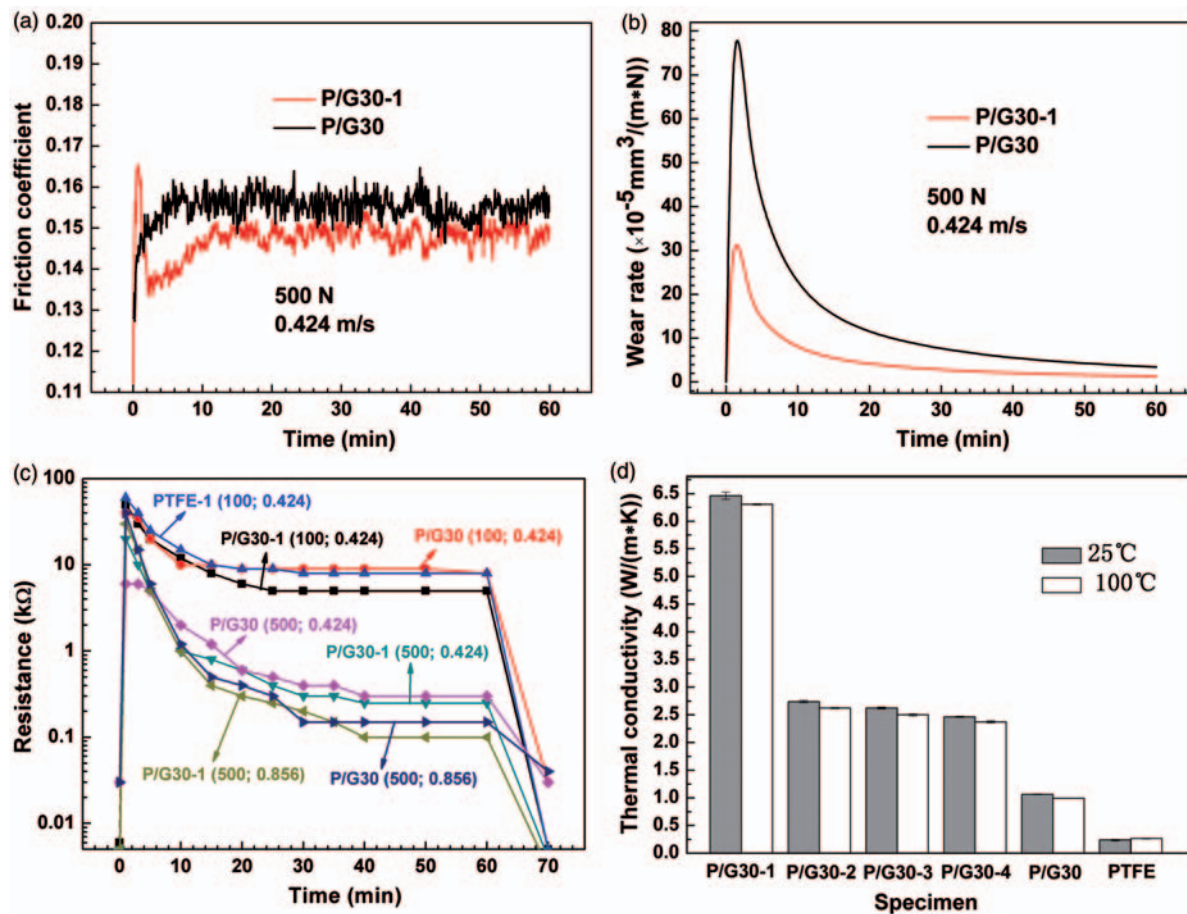
Fig. 9 Variations of the (a) friction coefficients at a velocity of 0.424 m/s at a load of 500 N; (b) wear rates at 0.424 m/s at 500 N; (c) contact resistances at linear velocities of 0.424 and 0.856 m/s at loads 100 and 500 N; and (d) values of the thermal conductivity of specimens at 25°C and 100°C (P/G30: 70% PTFE + 30% graphite; P/G30-1: foamed copper 1# filled with P/G30 component; P/G30-2: foamed copper 2# filled with P/G30 component, and so on)

its composites have the nature of mechanical relaxation and viscoelasticity. The strain hysteresis (a phase lag) occurs for a dissipation of mechanical energy when cyclic loading is applied [**24**]. For the FCB composites, the stick-slip motion of the friction pairs and the vibration of test machine provide the cyclic loading. When the velocity of the ring becomes higher, the cyclic strain of polymer is observed to lag behind the stress caused by the loading force. This will lead to the development of cavities and the high-speed stick-slip of the rubbing pairs before the strain matched the stress. The area and depth of contact on the frictional interface correspondingly decrease owing to the strain hysteresis. Hence, the friction coefficients of the FCB composites decrease at higher values of velocity. The friction coefficients of polymer P/G20 and P/G30 are insensitive to the velocity because the strain hysteresis of polymer is also influenced by temperature. The homologous polymer is inefficient on the dissipation of friction heat and

the higher temperature increases the viscosity coefficients of polymer. The high viscosity depresses the strain hysteresis of polymer, so that the friction coefficient of homologous polymer changes little.

3.2.4 *Variations of the friction coefficients and wear rates of specimens with sliding duration*

Figures 9(a) and (b) shows some typical variations in the friction coefficients and wear rates of the specimens P/G30-1 and P/G30 at 0.424 m/s at an applied load 500 N during the sliding time. It can be seen from Fig. 9(a) that the fluctuations of friction coefficients are similar in the sliding time. Figure 9(b) shows the variations of wear rates with sliding duration. The curves of wear rates have dramatically changing beginnings and flat subsequent areas, and the results show that the character of wear rate is mostly consistent with that of friction coefficient.

Typically, at the beginning of the running-in stage, the local direct contact between the copper and steel ring results in a higher friction coefficient. Following that, the lubricating film formed by the solid lubricant of high expansion coefficient quickly and ceaselessly intervenes in the frictional interface, and the plastic deformation or fracture of 'platelets' of lubricants leads to compaction, causing rapid decrease in the friction coefficient. The formation process of lubricating film simultaneously corresponds to the high wear rate. As the temperature in frictional interface rises, the formation and stripping of lubricating film come to a new dynamic equilibrium at the end of the breaking-in stage, and then the wear enters the steady stage.

3.2.5 Variations of the contact resistances of specimens with sliding duration

Figure 9(c) shows the variation tendency of DC contact resistance of each selective specimen under different conditions. The tendency of contact resistance is substantially consistent with that of wear rate for the contact resistance is inversely related to the contact area. It is at some local convex points and/or facets named as contact spots that the transfer layers would contact each other and form a higher conductivity network within the contact zone of the steel ring and the FCB composite. The contact spots consist of dielectric/conducting film and wear debris. Here, when the thickness of lubricating film is below a critical value (approximately 2 nm), the film can be conductive owing to the tunnelling effect [26]. A further study on the values of the contact resistances indicates that the frictional interface layer has a higher resistance at the wear stage, while the contact resistance is relatively smaller before and after the run. The higher resistance at the wear stage is due to the fact that as the friction begins, the lubricants quickly move into the interface by the thermal expansion of PTFE matrix; and then the area and depth of contact on the frictional interface correspondingly decrease owing to the strain hysteresis of polymeric composite described above. The larger applied load corresponds to smaller contact resistance owing to the increase of contact area. The higher sliding velocity 0.856 m/s reduces the value of contact resistance a little, for which the reason considered is that for the polymer P/G30, the plastic deformation caused by higher friction heat increases the actual contact area; and for the FCB composite P/G30-1, the conducting wear debris, such as copper and graphite, in the active transfer layer contributes to the smaller contact resistance despite the strain hysteresis of polymeric composite.

3.2.6 Thermal conductivity and friction heat analysis

Figure 9(d) shows the comparison of the thermal conductivity values of the composites P/G30 series and PTFE at 25°C and 100°C. It can be observed that the thermal conductivity is greatly improved owing to the existence of foamed copper. The thermal conductivity of P/G30 is more than 20 times of pure PTFE. Additionally, the thermal conductivity of each of the P/G30 series specimens is slightly lower at 100°C than that at 25°C except pure PTFE. This behaviour indicates that the FCB composites are effective in transmitting and dissipating heat.

Figure 10 shows the values of the temperature of P/G30 Series specimens each at three temperature measuring points and variations of temperature with sliding duration at the location of 1.8 mm at a velocity of 0.424 m/s at a load of 500 N. It is observed that the interfacial friction temperatures of FCB composites are generally lower than the one without foamed copper when the measurement is close to the frictional surfaces. Temperatures fall more slightly owing to the copper struts when the measurement is far from the interface (Fig. 10(a)). Although the copper strut in the friction surface is the heat source, a balance between heat generation and dissipation still can be seen in the friction process owing to good thermal conductivity along with the sliding (Fig. 10(b)).

3.4 Wear mechanism analysis

The above tests show that, of all the specimens, the P/G30-1 exhibits the highest wear resistance in the sliding time in spite of its slightly higher friction coefficients at some lower loads. This behaviour can be attributed to the presence of graphite flakes and the foamed copper. Concretely, the graphite filled in both the FCB composites and the polymers without foamed copper act as an effective barrier to prevent large-scale fragmentation of PTFE. Several researchers have investigated the role of graphite as an effective filler material. Briscoe et al. [27] investigated the tribology behaviour of three carbons of differing particle shapes filled into the matrix of PTFE, and proposed that the interfacial temperature relevant to the thermal conductivity of the composite and stresses at local regions were very important factors for the net adhesion of the transferred film to the counterface. Bijwe et al. [28] pointed out that the filler graphite particles increased abrasive wear, which was attributed to the reinforcement greatly reducing the ultimate elongation to fracture in
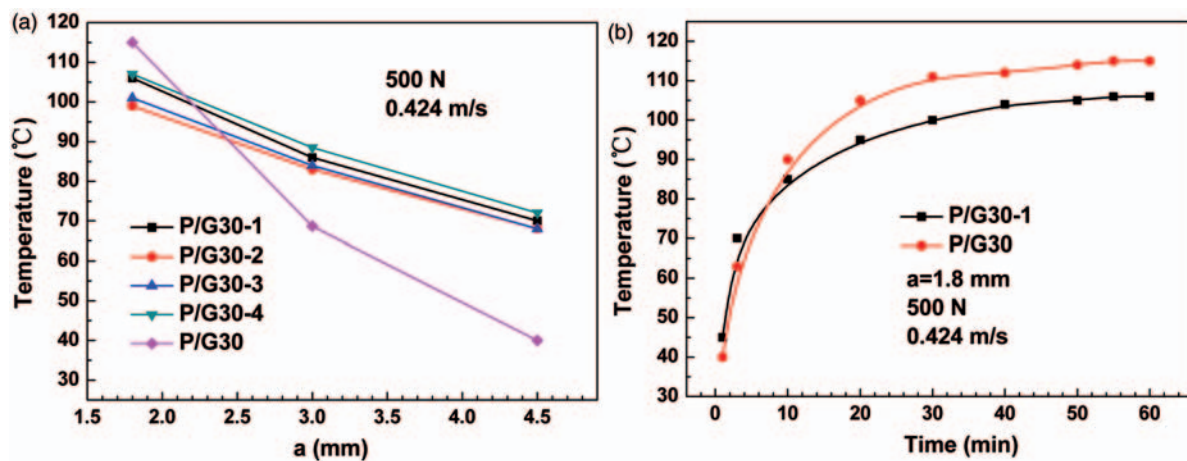
Fig. 10 Values of the temperature of specimens each at three temperature measuring points (a) and variations of temperature with sliding duration at the location of 1.8 mm (b) at a velocity of 0.424 m/s at a load of 500 N (P/G30: 70% PTFE + 30% graphite; P/G30-1: foamed copper 1# filled with P/G30 component; P/G30-2: foamed copper 2# filled with P/G30 component, and so on)
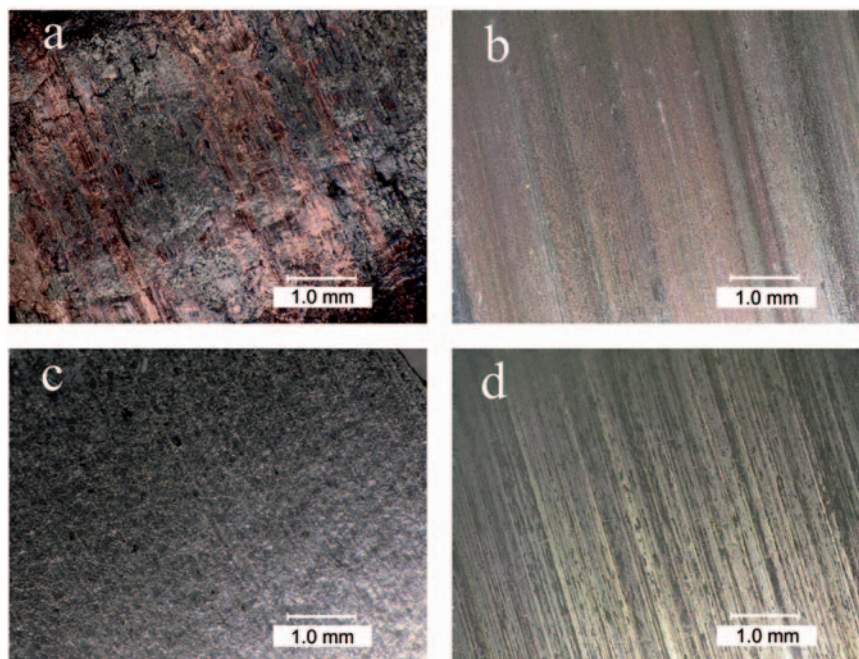

Fig. 11 Optical micrographs (50×) of worn surfaces of composites (left column) and steel rings (right column) of (a, b) P/G30-1 at 0.856 m/s and (c, d) P/G30 at 0.856 m/s at a load of 500 N (P/G30: 70% PTFE + 30% graphite; P/G30-1: foamed copper 1# filled with P/G30 component)

abrasive wear performance. Optical micrographs of Fig 11(a) and (b) show the worn surfaces of composites P/G30-1 and counterpart steel rings at 0.856 m/s at a load of 500 N. As a contrast, the worn surfaces of P/G30 at 0.856 m/s at 500 N are shown in Figs 11(c) and (d). The plastic deformation and adhesion of the malleable copper on the surface of the FCB composites after sliding are evidently shown.

Figures 12 and 13 show the optical and SEM micrographs of the worn surfaces of P/G30-1 and P/G30 at 0.424 m/s at 500 N, respectively. A copper–polymer interfacial transition zone is shown in Figs 13(a) and (b), and the worn surface of FCB composite can be divided into three areas with the visible copper struts: transitional, hollow metallic strut, and polymer. It is seen that the wear scar on the hollow
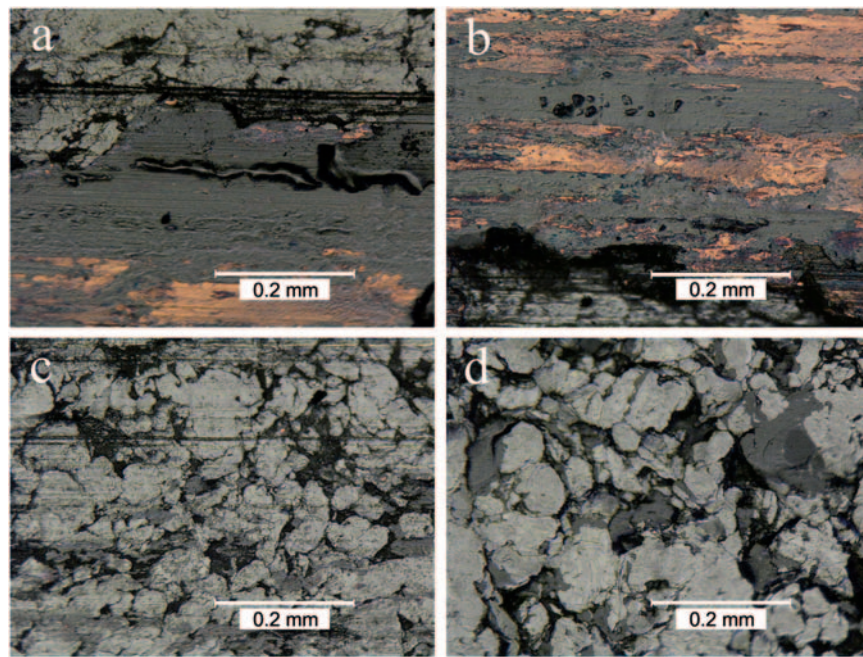
Fig. 12 Optical micrographs (500×) of the worn surfaces of composite P/G30-1 (a, b, and c) and the polymer composite P/G30 (d) at 0.424 m/s at a load of 500 N (P/G30: 70% PTFE + 30% graphite; P/G30-1: foamed copper 1# filled with P/G30 component)
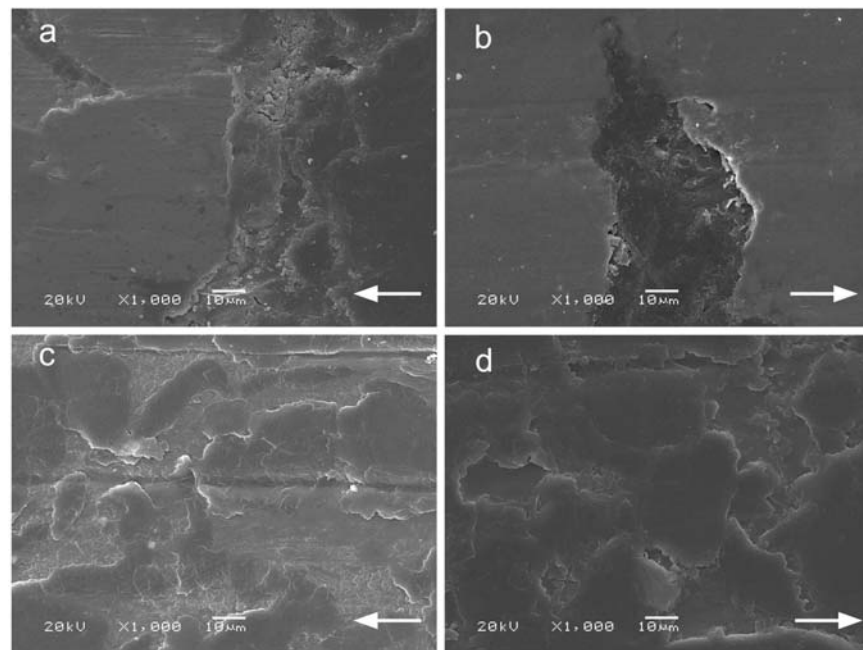

Fig. 13 SEM micrographs of the worn surfaces of composite P/G30-1: (a) transitional area, (b) hollow metallic strut, and (c) polymer area, and the polymer composite P/G30 (d) at 0.424 m/s at a load of 500 N (the sliding direction is shown by arrows; P/G30: 70% PTFE + 30% graphite; P/G30-1: foamed copper 1# filled with P/G30 component)

metallic strut is smoother and shows less apparently plucked and ploughed marks than the polymer area, except for the cavity shown in the matrix. These cavities belong to the hollow copper struts, and can serve for collecting and storing lubricants in interfacial

friction. The worn surfaces on the polymer areas of the two composites are not much different except for some marks of hard particle erosion and plastic furrow deformation (Figs 12(c) and (d) and 13(c) and (d)). Material flow can be clearly seen along the
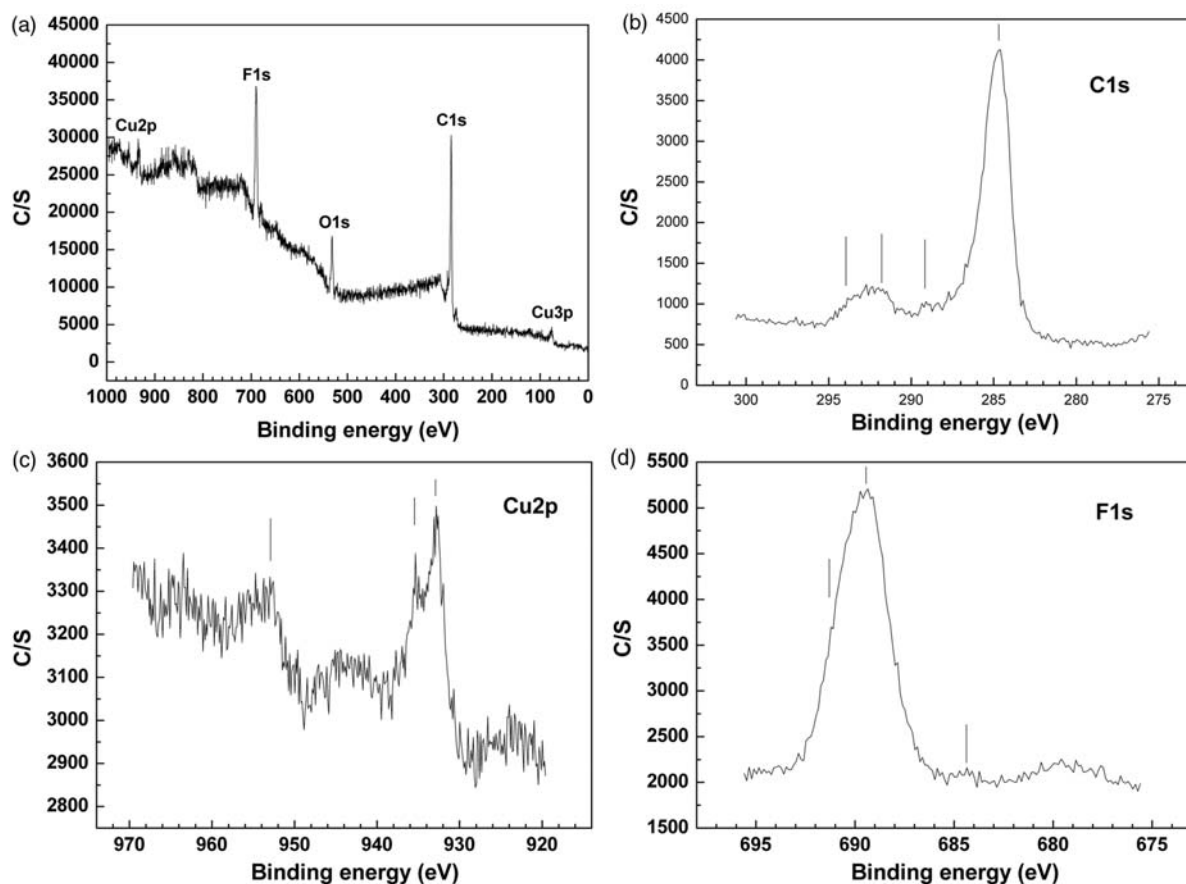
Fig. 14 XPS spectra of the transfer film on the copper-colour area of composite P/G30-1: (a) the full spectrum; (b) C1s; (c) Cu2p; and (d) F1s at a velocity of 0.424 m/s at a load of 500 N (P/G30-1: foamed copper 1# filled with P/G30 component)

sliding direction through the contacting surface layer (Fig. 13). Also, it is the material flow that could tend to partially or fully cover up the existing porosity. It is the friction heat, compressive stress, and tensile stress that originate and extend the polymer flow. Figure 14 shows the X-ray photoelectron spectroscopy (XPS) image on the specific region of transfer film of composite P/G30-1 where the copper strut is visible to determine the role of foamed copper in the formation of the composite transfer film. The worn PTFE have almost the same peaks of C1s and F1s as the pure unworn one. This indicates that no apparent tribochemical reactions occurred for the PTFE in sliding against the steel ring. The amount of radical – CF_3 generated on the surface of PTFE composites mentioned by Li et al. [29] is extremely small; for the C1s peak at 294.20 eV and F1s peak at 691.6 eV, they are insignificant, as shown in Figs 14(b) and (d). The potential F1s peak at 684.5 eV, which indicates the iron fluoride bonds mentioned by Voort and Bahadur [30] is also very little and the Fe2p spectrum is nearly invisible in the full spectrum. The main peak in the Cu2p spectrum at 932.8 eV corresponds to

copper (Cu) and its oxides (Cu_2O and CuO), as verified from the Cu3p peak at 75.8 eV and Cu2p peak at 952.9 eV in Figs 14(a) and (c). The smaller peak at 935.3 eV corresponds to $Cu_2CO_3(OH)_2$ supported by the C1s peak at 289.1 eV shown in Fig. 14(b).

The above XPS results reveal that during the sliding process, the oxidation of copper is the dominant chemical process which occurred. The elements carbon and fluorine on the visible copper-colour area verify the presence of the composite transfer film; and the oxides (Cu_2O and CuO) also promote and enhance the adhesion of the transfer films to the steel surface.

Figure 15 shows the schematic representation of the wear mode of the FCB composite during sliding duration. The actual contact form is shown in Fig. 15(a). The abrasion mechanism in the process is a three-body phenomenon. The mechanism is caused and promoted by the plastic deformation, abrasive wear, and fatigue spalling [31]. The composition of wear debris on the contact surface includes copper debris (the oxides included), graphite debris, and PTFE debris. This wear debris between the transfer
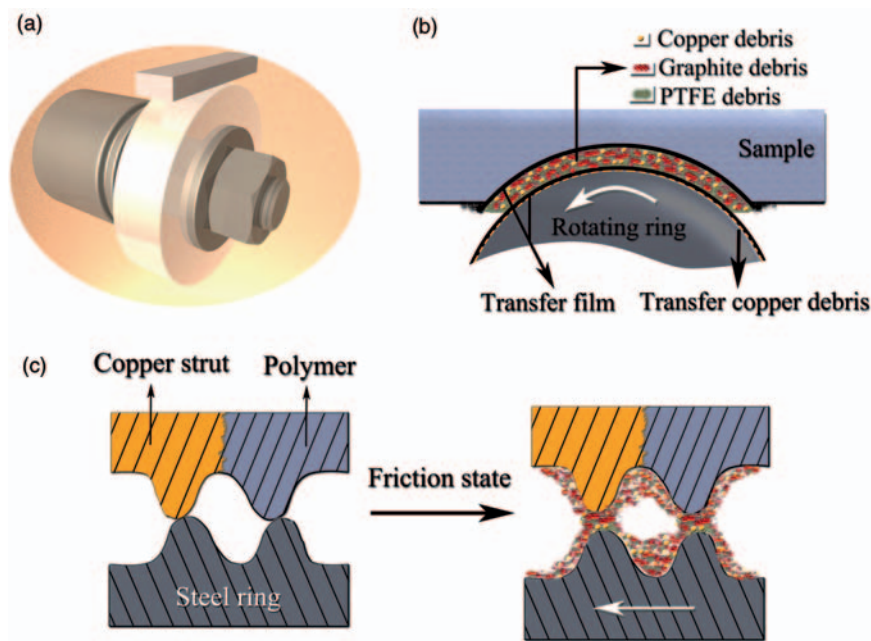
Fig. 15   Schematic representation of the wear mode of the FCB composite during sliding duration: (a) actual contact form; (b) wear mode and the composition of wear debris on the contact surface; and (c) the friction process simulation (thickness exaggerated)

films keeps a balanced state of accumulation and extrusion. The debris squeezed out by the rotating ring piles up on the outlet are shown on the left of Fig. 15(b), while the debris peeled off by the sample piles up at the entrance are shown on the right of Fig. 15(b). The friction process simulation is shown in Fig. 15(c). The sample and ring surfaces directly contact before the run, and some contact spots made of copper contribute to the higher conductivity network within the contact zone of the steel ring and the FCB composite. Noticing friction, the lubricants quickly move into the interface, which is in accordance with the variation tendency of contact resistance. The copper debris coming from the foamed copper strut serves as abrasive and conductive particles. This debris would be abrasive to intact transferred film derived from copper strut, pulled and dragged by shear force under sliding. Due to the abrasive nature of the copper embraced by polymer, it indicated a strong possibility of abrasive wear and furrow wear at the initial period of wear, where the sharp copper struts and particles scraped by friction ploughed the matrix of the polymer and the transfer film formed on the counterface. As the friction continued, the heat increases in local regions, leading to plastic deformation, adhesive wear, and fatigue spalling, which play a dominant role on the frictional interface, and the copper debris partly transfers to the ring surface. This transfer of copper debris improves the adhesion of the film, and the higher the sliding velocity and the applied load, the more apparent this trend became.

4   CONCLUSIONS

Four kinds of foamed copper samples ppi 10–28, porosities of 93–98 per cent, were filled inside with solid lubricants such as PTFE and graphite effectively with the help of vacuum filtration apparatus in this study. On the basis of the results presented, the following conclusions can be formulated.

1. The FCB composites exhibit outstanding thermal and electrical conductivities owing to the interconnected metal skeletons embedded in the polymers.
2. The wear rates of FCB composites substantially decrease compared with those of the homologous polymers. The friction coefficients of the FCB composites decrease almost monotonically with the increase of graphite content. To achieve better tribological properties, the optimal graphite content is 20 per cent for the homologous polymers and 30 per cent for the FCB composites. The preferable wearing quality especially under severe mode benefits from the favourable thermal conduction and the hollow metallic struts of the foamed copper. The adhesion of copper debris to frictional interfaces also promotes the formation of transfer film and improves the adhesion of the film.
3. The study on the contact resistances indicates that owing to the strain hysteresis of polymeric composite, the frictional interface layer has a higher resistance at the wear stage, while the contact resistance is relatively smaller before and after the run. The contact spots within transfer layer

consist of dielectric/conducting film and wear debris. Also, the conducting wear debris includes the copper debris (its oxides included) and graphite debris in the active transfer layer.

4. XPS analysis results on the visible copper-colour area show that the oxidation of copper is the dominant chemical process which occurred during the sliding process. The elements carbon and fluorine verify the presence of the composite transfer film.

5. The abrasion mechanism of the FCB composites in the process is a three-body phenomenon. The mechanism is caused and promoted by the plastic deformation, abrasive wear, and fatigue spalling.

FUNDING

ACKNOWLEDGEMENTS

REFERENCES

1 **Chan, D.** and **Stachowiak, G. W.** Review of automotive brake friction materials. *Proc. IMechE, Part D: J. Automobile Engineering*, 2004, **218**, 953–966.

2 **Feng, Y., Zhang, M.,** and **Xu, Y.** Effect of the electric current on the friction and wear properties of the CNT-Ag-G composites. *Carbon*, 2005, **43**, 2685–2692.

3 **Khoddamzadeh, A., Liu, R.,** and **Wu, X. J.** Novel polytetrafluoroethylene (PTFE) composites with newly developed Tribaloy alloy additive for sliding bearings. *Wear*, 2009, **266**, 646–657.

4 **He, J. Q., Zhang, L.,** and **Li, C. Z.** Thermal conductivity and tribological properties of POM-Cu composites. *Polym. Eng. Sci.*, 2010, **50**, 2153–2159.

5 **Sun, X. L., Liu, Y.,** and **Lu, Y.** P/M metal-matrix high-temperature solid self-lubricating materials. *Powder Metall.*, 2001, **19**, 86–92.

6 **Liu, Z. M.** Elevated temperature diffusion self-lubricating mechanisms of a novel cermet sinter with orderly micro-pores. *Wear*, 2007, **262**, 600–606.

7 **Pelletiers, T., Nadkarni, A., Ijeoma, R.,** and **Murphy, T.** Improving performance from self-lubricating bronze bearings. *Met. Powder Rep.*, 2007, **62**, 26–31.

8 **Kim, J. H., Kim, R. H.,** and **Kwon, H. S.** Preparation of copper foam with 3-dimensionally interconnected spherical pore network by electrodeposition. *Electrochem. Commun.*, 2008, **10**, 1148–1151.

9 **Sanz, O., Echave, F. J., Sanchez, M., Monzon, A.,** and **Montes, M.** Aluminium foams as structured supports for volatile organic compounds (VOCs) oxidation. *Appl. Catal., A*, 2008, **340**, 125–132.

10 **Banhart, J.** and **Weaire, D.** On the road again: metal foams find favor. *Phys. Today*, 2002, **55**, 37–42.

11 **Qu, J., Blau, P. J., Klett, J.,** and **Jolly, B.** Sliding friction and wear characteristics of novel graphitic foam materials. *Tribol. Lett.*, 2004, **17**, 879–886.

12 **Wang, Y. J.** and **Liu, Z. M.** Tribological properties of high temperature self-lubrication metal ceramics with an interpenetrating network. *Wear*, 2008, **265**, 1720–1726.

13 **Blanchet, T. A., Kandanur, S. S.,** and **Schadler, L. S.** Coupled effect of filler content and countersurface roughness on PTFE nanocomposite wear resistance. *Tribol. Lett.*, 2010, **40**, 11–21.

14 **Akdogan, G., Stolarski, T. A.,** and **Tobe, S.** Wear performance of polytetrafluoroethylene-metal coatings in rolling/sliding line contact. *Proc. IMechE, Part J: J. Engineering Tribology*, 2003, **217**, 103–114.

15 **Khedkar, J., Negulescu, I.,** and **Meletis, E. I.** Sliding wear behavior of PTFE composites. *Wear*, 2002, **252**, 361–369.

16 **Sawyer, W. G., Freudenberg, K. D., Bhimaraj, P.,** and **Schadler, L. S.** A study on the friction and wear behavior of PTFE filled with alumina nanoparticles. *Wear*, 2003, **254**, 573–580.

17 **Gódor, I., Major, Z., Vezér, S.,** and **Grün, F.** Experimental definition of a failure model for the tribological behavior of polytetrafluoroethylene bronze compounds. *Proc. IMechE, Part J: J. Engineering Tribology*, 2009, **223**, 807–815.

18 **Cheng, X. H., Shang, G.,** and **Qian, Q.** Effect of rare earths on mechanical and tribological properties of carbon fibers reinforced PTFE composite. *Tribol. Lett.*, 2006, **23**, 93–99.

19 **McCook, N. L., Burris, D. L., Bourne, G. R., Steffens, J., Hanrahan, J. R.,** and **Sawyer, W. G.** Wear resistant solid lubricant coating made from PTFE and epoxy. *Tribol. Lett.*, 2005, **18**, 119–124.

20 **Wang, H. L., Li, H. H.,** and **Yan, F. Y.** Synthesis and tribological behavior of metakaolinite-based geopolymer composites. *Mater. Lett.*, 2005, **59**, 3976–3981.

21 **Piljavskij, V. S.** Heat sources localization at external friction of metals. *Sov. J. Frict. Wear*, 1991, **12**, 33–38.

22 **Abdel-Aal, H. A.** On the bulk temperatures of dry rubbing metallic solid pairs. *Int. Commun. Heat Mass Trans.*, 1999, **26**, 587–596.

23 **Burris, D. L.** and **Sawyer, W. G.** Hierarchically constructed metal foam/polymer composite for high thermal conductivity. *Wear*, 2008, **264**, 374–380.

24 **Wieleba, W.** The role of internal friction in the process of energy dissipation during PTFE composite sliding against steel. *Wear*, 2005, **258**, 870–876.

25 **Yan, F. Y., Xue, Q. J.,** and **Yang, S. R.** Debris formation process of PTFE and its composites. *J. Appl. Polym. Sci.*, 1996, **61**, 1223–1229.

26 **Myshkina, N. K.** and **Konchits, V. V.** Evaluation of the interface at boundary lubrication using the measurement of electric conductivity. *Wear*, 1994, **172**, 29–40.

27 **Briscoe, B. J., Steward, M. D.,** and **Groszek, A. J.** The effect of carbon aspect ratio on the friction and wear of PTFE. *Wear*, 1977, **42**, 99–107.

28 **Bijwe, J., Logani, C. M.,** and **Tewari, U. S.** Influence of fillers and fibre reinforcement on abrasive wear resistance of some polymeric composites. *Wear*, 1990, **138**, 77–92.

29 **Li, F., Yan, F. Y., Yu, L. G.,** and **Liu, W. M.** The tribological behaviors of copper-coated graphite filled PTFE composites. *Wear*, 2000, **237**, 33–38.

30 **Voort, J. V.** and **Bahadur, S.** The growth and bonding of transfer film and the role of CuS and PTFE in the tribological behavior of PEEK. *Wear* 2000, 181–183, 212–221.

31 **Briscoe, B. J.** and **Sinha, S. K.** Wear of polymers. *Proc. IMechE, Part J: J. Engineering Tribology*, 2002, **216**, 401–413.